

SUPPLEMENTARY INFORMATION

**Protein Adsorption and Transformation on Catalytic and Food-Grade TiO₂
Nanoparticles in the Presence of Dissolved Organic Carbon**

Junyeol Kim^a and Kyle Doudrick^{a*}

^aDepartment of Civil and Environmental Engineering and Earth Sciences, University of Notre
Dame, Notre Dame, Indiana, USA, 46637

***Corresponding Authors and Address:**

Kyle Doudrick*, Department of Civil and Environmental Engineering and Earth Sciences
, University of Notre Dame, Notre Dame, Indiana, USA, 46637

e-mail: kdoudrick@nd.edu

Table S1. Secondary structure in the amide I band of BSA and their assigned wavenumbers for curve fitting analysis. ¹⁻⁵

Assigned secondary structure	Wavenumber range (cm ⁻¹)
β-sheets	1690–1700
β-sheets/β-turns	1685–1663
α-helices	1665–1650
Random chains	1648–1644
Extended chains/β-sheets	1639–1621
Side chain moieties	1616–1600

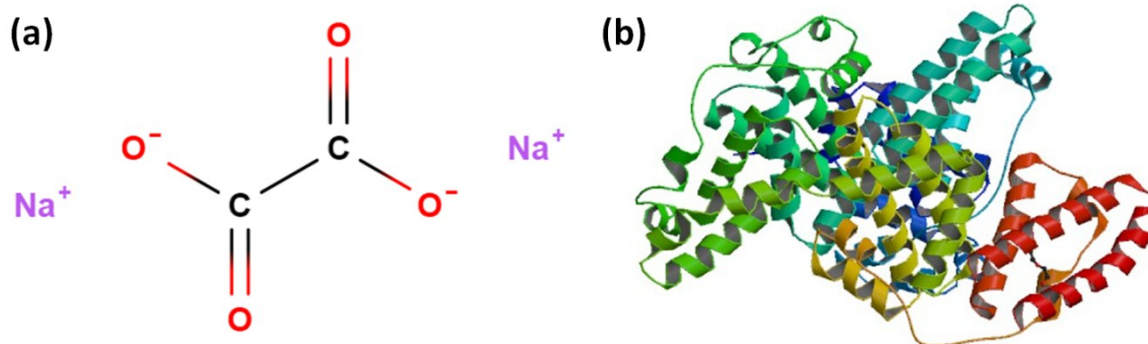


Figure S1. The molecular structure of sodium oxalate (a) and BSA (b). BSA structure was obtained from <http://www.rcsb.org/structure/4F5S>

Diffuse reflectance infrared Fourier transform spectroscopy (DRIFTS; Bruker Vertex 70) and X-ray photoelectron spectroscopy (XPS; PHI VersaProbe II) were used to characterize the surface composition of P90 and E171. Results from the DRIFTS analysis showed that phosphate peaks (1151 and 1072 cm⁻¹) were present for E171 but no P90. (Fig.

S2).

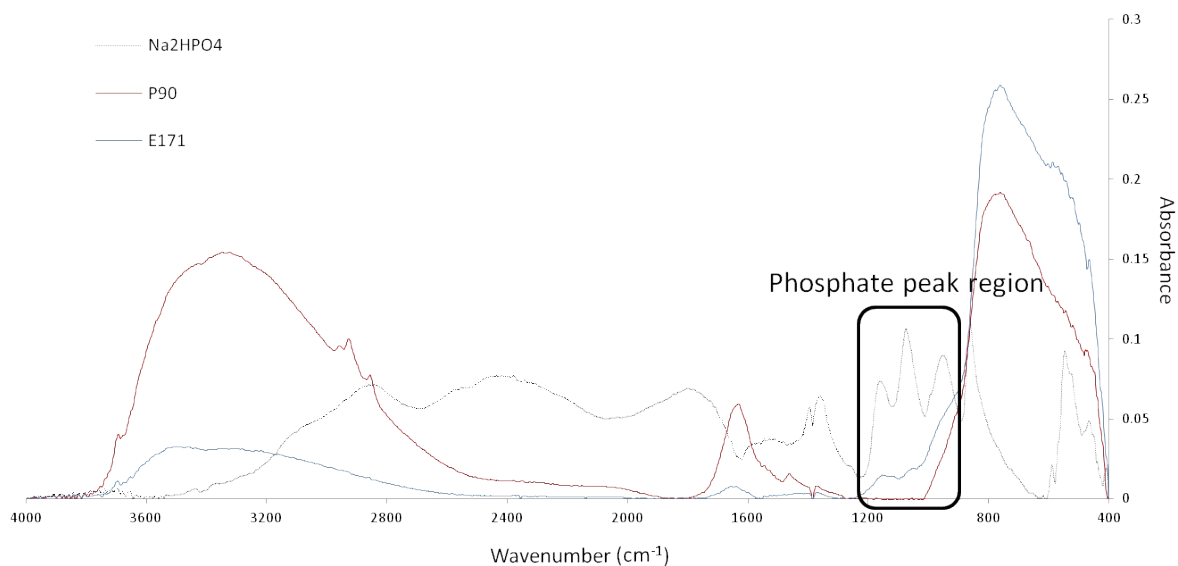


Figure S2. DRIFT peaks of P90, E171, and Na₂HPO₄ (control).

XPS scans of the phosphorous 2p region (128-138 eV) were performed for E171 and P90 powders. All spectra were normalized to the C 1s emission (284.6 eV) and fit using relevant software. XPS analysis of the phosphorous 2p region for P90 (Fig. S3(a)) showed that phosphorus was not present on the surface. Conversely, the XPS spectra of E171 (Fig. S3(b)) showed a major peak at 133.0 eV, which is consistent with the peak location of the 2p_{3/2} orbital of metal phosphates. The atomic mass percent of phosphorus measured on the E171 sample was approximately 2.9%.

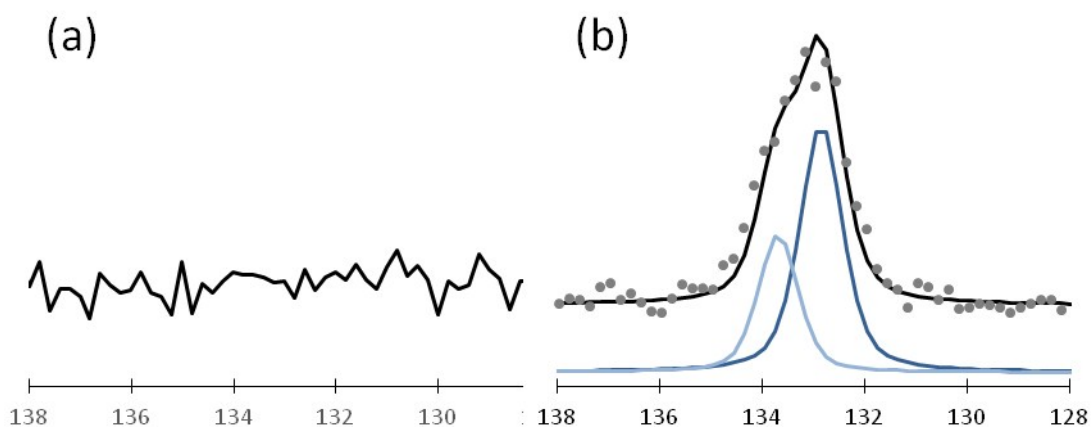


Figure S3. XPS analysis of the phosphate $2p_{3/2}$ orbital of (a) P90 and (b) E171

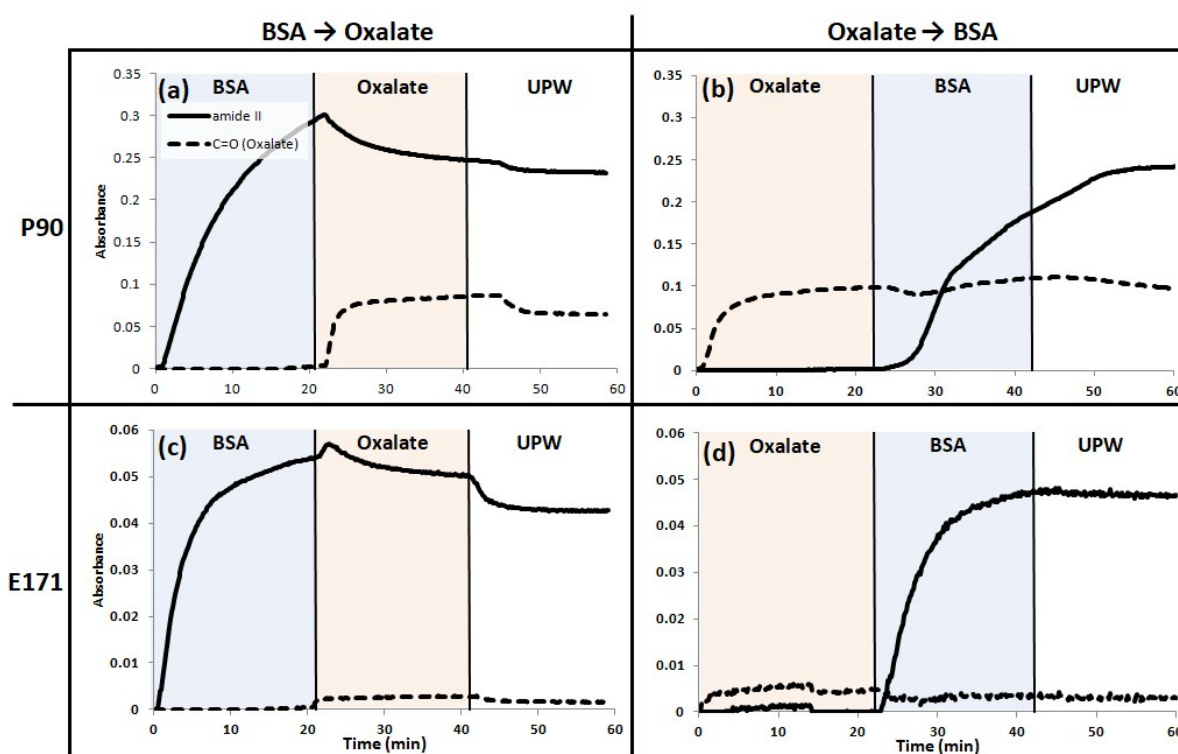
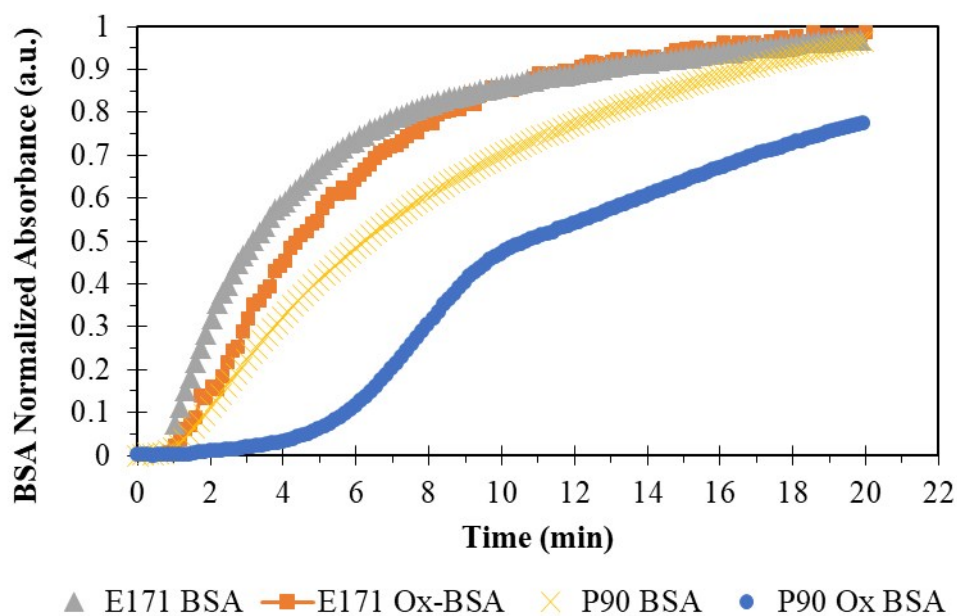


Figure S4. Flow-through ATR-FTIR spectra (64 scans, 4 cm^{-1}) comparing the maximum peak intensities of BSA in the presence and absence of pre-formed oxalate layers on P90 (a, b) and E171 (c, d) film. Amide II (1547 cm^{-1}) and C=O (1693 cm^{-1} and 1699 cm^{-1} for P90 and E171, respectively) peaks were used for the comparison.

(a)



(b)

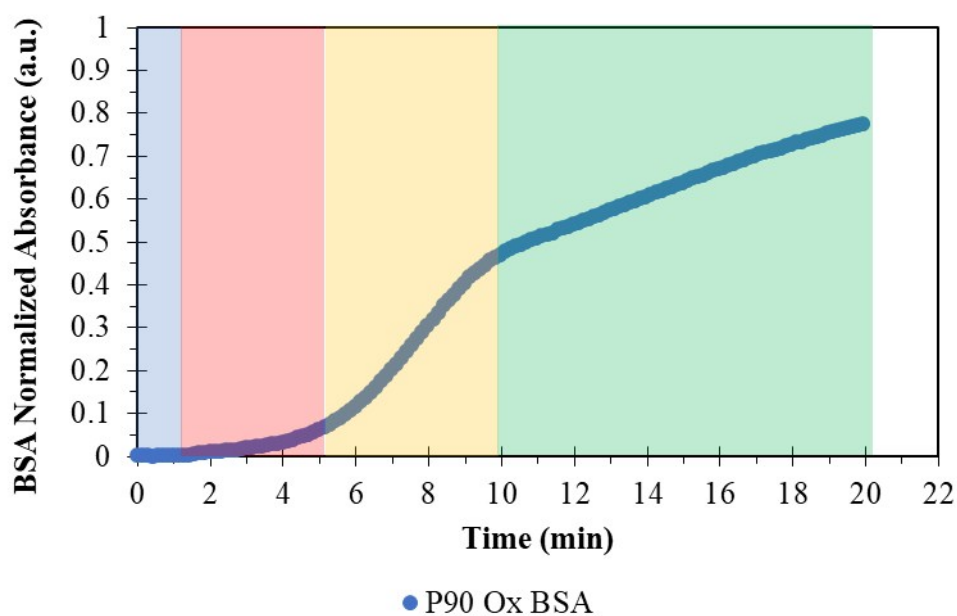


Figure S5. Flow-through ATR-FTIR spectra (64 scans, 4 cm^{-1}) of (a) a comparison of adsorption kinetics of BSA onto P90 and E171 in the presence and absence of pre-adsorbed oxalate, and (b) distinct kinetic regions of BSA sorption to P90 in the presence of pre-adsorbed oxalate.

Table S2. Hydrodynamic size and zeta potential of P90 and E171 in the presence of BSA and/or oxalate and 1 mM KNO₃. The Smoluchowski model was used to determine zeta potential.

		TiO ₂	TiO ₂ + BSA	TiO ₂ + OX	TiO ₂ + BSA + OX
P90	pH	4.71	4.60	6.43	5.92
	Size (nm)	279 ± 3.4	1116 ± 75.6	2112 ± 167	302 ± 4.2
	ζ potential (mV)	6.7 ± 0.3	-0.8 ± 0.4	-7.2 ± 0.5	-2.8 ± 0.7
E171	pH	5.85	5.04	6.62	5.92
	Size (nm)	315 ± 9.9	464 ± 0.3	338 ± 7.2	378 ± 6.8
	ζ potential (mV)	-27.3 ± 2.9	-0.2 ± 0.8	-39.3 ± 2.8	-12.6 ± 0.8

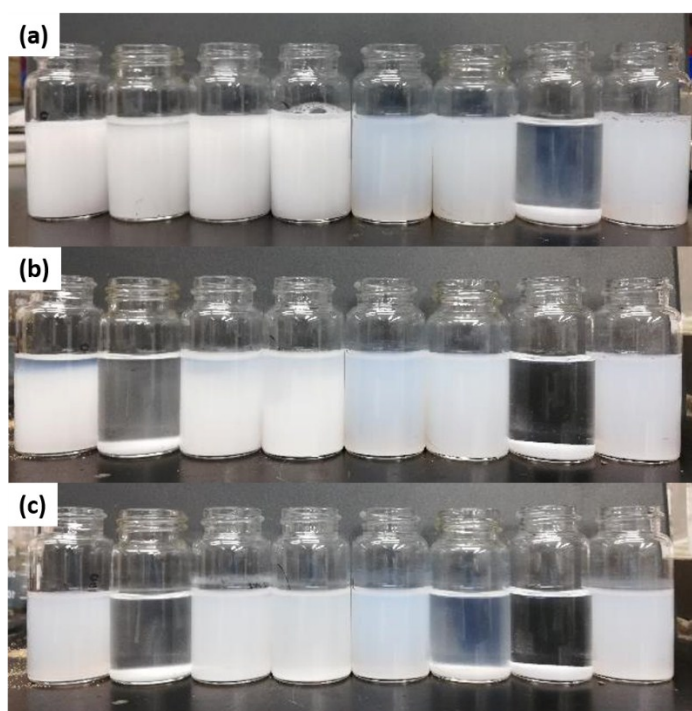


Figure S6. Changes in the stability of TiO₂ ENMs over time. (a) 2 hrs, (b) 12 hrs, and (c) 120 hrs after the initial interaction between TiO₂ NPs and BSA and/or OX. From the left to the right, the vials are: (1) E171, (2) E171 with BSA, (3) E171 with OX, (4) E171 with BSA and OX, (5) P90, (6) P90 with BSA, (7) P90 with OX, and (8) P90 with BSA and OX.

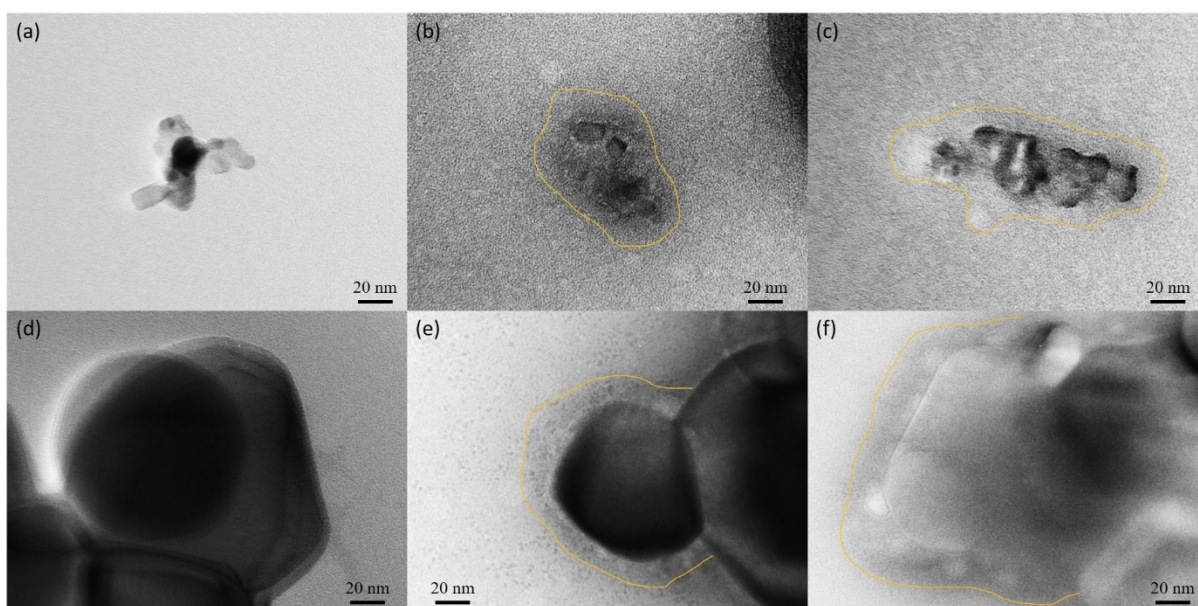


Figure S7. TEM images of TiO₂ ENMs in the presence and absence of BSA and/or OX. (a) P90, (b) P90 with BSA, (c) P90 with BSA and OX, (d) E171, (e) E171 with BSA, (f) E171 with BSA and OX. The scale bars on the bottom indicate 20 nm for all images. The yellow lines represent the approximate extent of the adsorbed layer. Due to aggregation, the adsorbed layer thickness of the P90 samples was not conclusive. The average primary particle diameter of the E171 samples in the presence of BSA increased from approximately 118 ± 30.5 to 164 ± 67.7 nm, a statistically significant increase ($p = 0.04$) for $n = 28$ and 12 particles measured, respectively. The p -value was calculated using a two-tailed t -test assuming unequal variance.

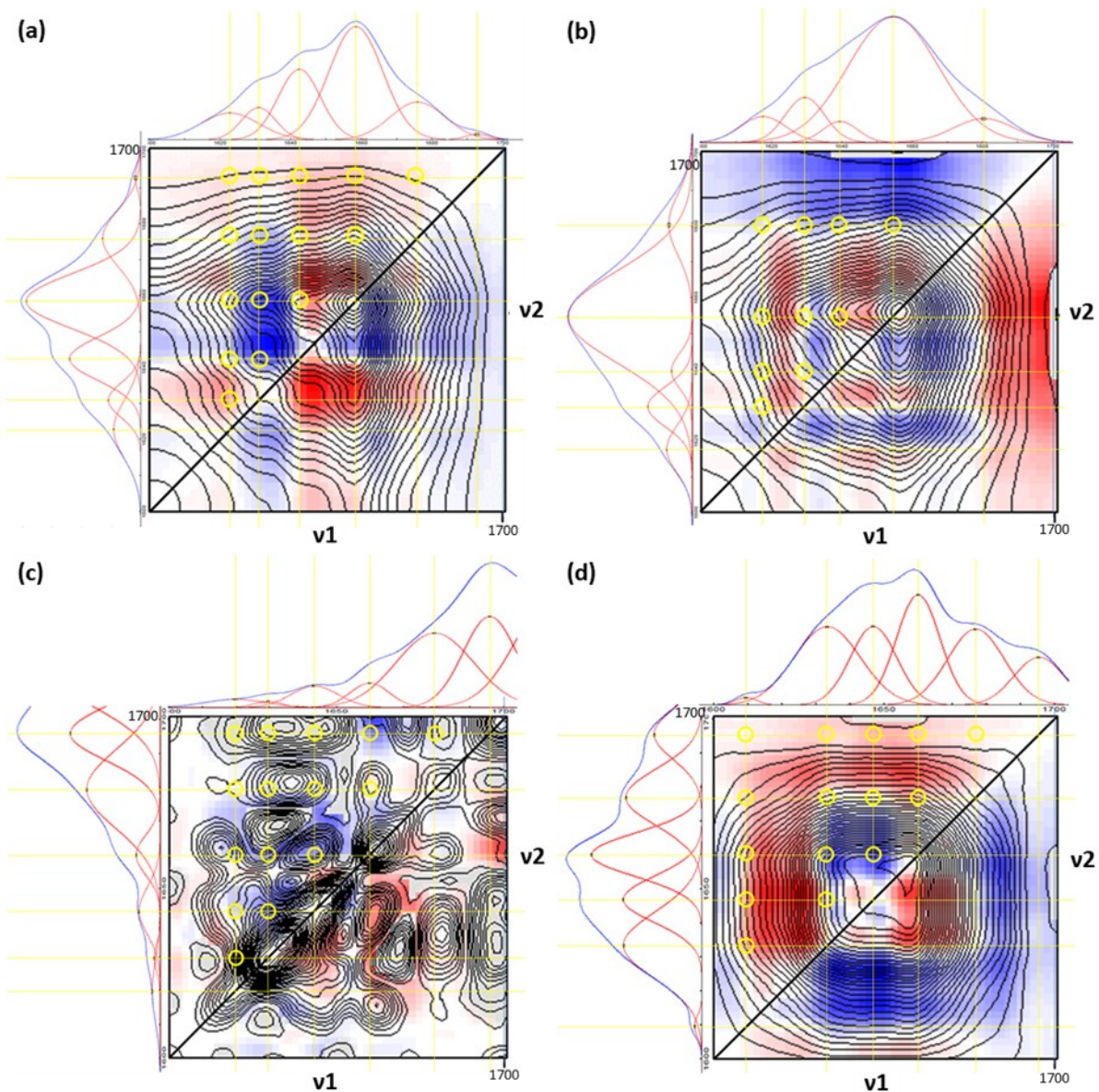


Figure S8. 2DCOS spectra of BSA secondary structures for (a) BSA on P90 film, (b) BSA on E171 film, (c) BSA on P90 film with oxalate pre-adsorbed, (d) BSA on E171 film with oxalate pre-adsorbed. Synchronous (contour lines) and asynchronous (red, blue) 2DCOS spectra are overlapped, and the synchronous spectra showed only positive values for BSA peaks except for (c).

REFERENCES

1. A. Barth, Infrared spectroscopy of proteins, *Biochimica et Biophysica Acta (BBA) - Bioenergetics*, 2007, 1767, 1073-1101.
2. B. E. Givens, Z. Xu, J. Fiegel and V. H. Grassian, Bovine serum albumin adsorption on SiO₂ and TiO₂ nanoparticle surfaces at circumneutral and acidic pH: A tale of two nano-bio surface interactions, *Journal of Colloid and Interface Science*, 2017, 493, 334-341.
3. P. Roach, D. Farrar and C. C. Perry, Interpretation of Protein Adsorption: Surface-Induced Conformational Changes, *Journal of the American Chemical Society*, 2005, 127, 8168-8173.
4. P. Roach, D. Farrar and C. C. Perry, Surface Tailoring for Controlled Protein Adsorption: Effect of Topography at the Nanometer Scale and Chemistry, *Journal of the American Chemical Society*, 2006, 128, 3939-3945.
5. Rustem I. Litvinov, Dzhigangir A. Faizullin, Yuriy F. Zuev and John W. Weisel, The α -Helix to β -Sheet Transition in Stretched and Compressed Hydrated Fibrin Clots, *Biophysical Journal*, 2012, 103, 1020-1027.